Optics Letters

Graphene-based metasurfaces for switching polarization states of anomalous reflection and focusing

Hua Zhu,[1] Shuqi Chen,[2] Jing Wen,[3] Jian Wang,[1] and Lin Chen[1,*]

[1]Wuhan National Laboratory for Optoelectronics, Huazhong University of Science and Technology, Wuhan 430074, China
[2]Laboratory of Weak Light Nonlinear Photonics Ministry of Education School of Physics, Teda Applied Physics Institute, Nankai University, Tianjin 300071, China
[3]Engineering Research Center of Optical Instrument and System, Ministry of Education and Shanghai Key Laboratory of Modern Optical System, University of Shanghai for Science and Technology, Shanghai 200093, China
*Corresponding author: chen.lin@mail.hust.edu.cn

Received 20 August 2019; revised 9 October 2019; accepted 11 October 2019; posted 11 October 2019 (Doc. ID 375839); published 27 November 2019

Metasurfaces have shown great potential to manipulate electromagnetic waves, and hence have found numerous applications in photonics. However, the functionalities of most of the reported metasurfaces are polarization unfriendly after the fabrication process and cannot be reconfigured dynamically with switchable polarization. Here, graphene-based metasurfaces are proposed to exhibit polarization-switchable electromagnetic response before and after switch of the chemical potential of graphene. The phase shifts covering a considerable phase range (with respect to 2π) can be switched from x polarization to y polarization by tuning the chemical potential of graphene from one value to another one. High-performance polarization-switchable anomalous reflection and focusing have been demonstrated with the designed metasurfaces. The presented design strategy can be applied to make other polarization-switchable metadevices in different frequency domains, and impact numerous photonic applications.

https://doi.org/10.1364/OL.44.005764

As two-dimensional equivalents of metamaterials, metasurfaces can provide full control of phase, amplitude, and polarization of electromagnetic waves (EWs), and hence have aroused extensive attention for developing various functional devices. Different from conventional optical devices that rely on refraction and propagation to reshape and control EWs, metasurfaces can impart control over the phase, polarization, and amplitude at deep-subwavelength scales. By properly tailoring the geometry of metasurface units, many alluring effects, such as anomalous reflection/refraction [1], focusing [2], optical orbital angular momentum generation [3], hologram [4], and so on, have been realized. Driven by application potential of EW manipulation related to polarizations, it is highly desirable to make metasurfaces operate with diverse polarizations. A variety of work on metasurfaces that operate with polarization dependence [5–7] and polarization independence [8,9] have been reported. However, most of the reported metasurfaces are passive, that is, the functionalities are polarization unfriendly after the fabrication process and cannot be reconfigured dynamically with switchable polarization [1–9].

Recent attention on metasurfaces has partially shifted to tunable, active, and reconfigurable metasurfaces. Such metasurfaces would enable unprecedented applications in modern optical systems, such as high-capacity communications, dynamic beam shaping, and real-time holograms. Tunable materials, including phase change materials [10], index tunable materials [11,12], liquid crystals [13,14], graphene [15,16], and liquid metals [17], have been used to realize active metasurfaces. Among these tunable metasurfaces, most of them are proposed to simply manipulate the phase, amplitude, and polarization of the emitted EWs [11,12,14,15]. Although liquid metal [17] and tunable capacitance/resistance [18] have been employed to construct active metasurfaces for the regulation of the emission phase of each unit in situ, and hence polarization-switchable wave-front manipulation is achievable in the microwave regime, it remains a significant challenge to extend these schemes to terahertz and higher frequencies. In this Letter, we have proposed a novel graphene metasurface to realize polarization-switchable wave-front control devices. Such metasurfaces are designed to exhibit polarization-switchable electromagnetic response before and after switch of the chemical potential of graphene. We can thus use such metasurfaces to realize desired polarization-switchable functionalities including anomalous reflection and focusing.

To construct polarization-switchable wave-front control devices, an anisotropic metasurface [shown in Fig. 1(a)] is designed to realize polarization-switchable electromagnetic response. Each unit contains two graphene blocks on the left and right sides of the unit cell [Fig. 1(b)], respectively, and the left- and right-side graphene blocks are termed as LGB and RGB, respectively. The graphene layer is covered with a layer of ion gel [Fig. 1(c)], which serves as gate dielectric having a high capacitance in graphene transistors. The graphene layer and ground gold film are

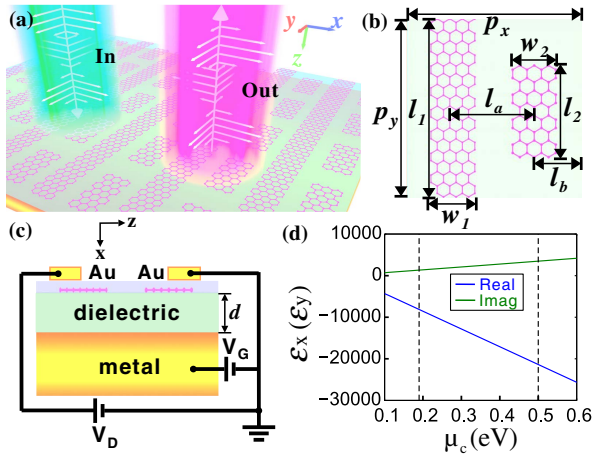

Fig. 1. (a) Schematic of the graphene metasurface. (b) Top view of a unit cell of the graphene metasurface. (c) Cross section of the metasurface unit cell. The periods of the unit cell along the x and y directions are denoted as p_x and p_y, respectively, and the length (width) of the LGB and RGB are defined as l_1 (w_1) and l_2 (w_2), respectively. The distance from the center of the RGB to the center of LGB and right-side boundary of the unit cell are denoted as l_a and l_b, respectively. The thickness of the dielectric spacer is d. Gold is selected as the metal layer with its relative permittivity described by the Drude model as $\varepsilon = \varepsilon_\infty - f_p^2/(f_\gamma + if_\gamma)$, where $f_p = 2069$ THz, $f_\gamma = 17.65$ THz and $\varepsilon_\infty = 1.53$ [19]. A loss-free poly tetrafluoroethylene (PTFE) is selected as the dielectric spacer, with its relative permittivity of 1.9 at THz frequencies [20]. (d) The real and imaginary parts of the in-plane permittivity of graphene versus μ_c occur at 1.5 THz. The two dashed vertical lines represent 0.19 and 0.50 eV, respectively.

separated by a dielectric spacer. The length of the LGB, l_1, is equal to p_y, namely, the LGB is infinitely long along the y direction. In this case, the y-polarized incidence does not allow the excitation of the surface plasmon resonance of the LGB, while the x-polarized incidence has the chance to excite the surface plasmon resonance with proper choice of w_1, with which the reflection phase of the x-polarized incidence can be significantly modulated. In contrast, the surface plasmon resonance of RGB can be excited by either x- or y-polarized incidence in principle, if l_2 or w_2 is suitably designed. Here, w_2 is set at a small value to avoid the response to x polarization with RGB, while l_2 can be varied within a large range to shift the reflection phase of the y-polarized incidence. It is highly desirable to enable LGB and RGB to work independently with the x and y polarizations, respectively.

In this work, all the simulation results are obtained with finite difference time domain (FDTD) method, computer software based on commercial solver *Lumerical FDTD Solutions*. In the simulations, graphene is characterized by its surface conductivity, described by the Kubo formula under the assumption of chemical potential, μ_c. In the infrared and terahertz frequencies, with $|\mu_c| \gg k_B T$ (k_B is Boltzmann constant, and T is the temperature), the surface conductivity of graphene could be approximated as

$$\sigma_g = \frac{ie^2 k_B T}{\pi\hbar^2(\omega + i\tau^{-1})}\left[\frac{\mu_c}{k_B T} + 2\ln\left(\exp\left(-\frac{\mu_c}{k_B T}\right) + 1\right)\right] + \frac{ie^2}{4\pi\hbar}\ln\left[\frac{2|\mu_c| - \hbar(\omega + i\tau^{-1})}{2|\mu_c| + \hbar(\omega + i\tau^{-1})}\right], \quad (1)$$

where e is the electron charge, $\hbar$ is the reduced Planck's constant, ω is the radian frequency, and τ is the momentum relaxation time representing the loss mechanism. In our study, $T = 300$ K, $\tau = 0.65$ ps. Considering that a DC mobility of $\mu > 100000$ cm^2 V^{-1} s^{-1} has been experimentally achieved in high-quality suspended graphene, which leads to $\tau > 1.5$ ps, our setting of $\tau = 0.65$ ps can reflect the practical transport loss of graphene conservatively. The effective in-plane permittivity of graphene can be written as

$$\varepsilon_x = \varepsilon_y = 1 + \frac{i\sigma_g \eta_0}{k_0 d_g}, \quad (2)$$

where $\eta_0 (= 377\Omega)$ is the impedance of air, k_0 is the wave vector in the air, and $d_g (= 0.34$ nm) is the thickness of graphene. The real and imaginary parts of the in-plane permittivity of graphene versus μ_c are shown in Fig. 1(d), while the out-of-plane permittivity of graphene, ε_z, is kept constant at 2.5, regardless of the Fermi level.

Here, two values of μ_c are chosen to realize the functionalities described as follows. When μ_c is set to be the first value, the reflection phase of the x-polarized incidence should be able to realize full 2π coverage by changing w_1, while the reflection phase of the y-polarized incidence should be kept nearly unchanged by changing l_2; In contrast, if μ_c is switched to another value, the reflection phase of the y-polarized incidence should realize full 2π coverage by changing l_2, while the reflection phase of the x- polarized incidence should be kept nearly unchanged by varying w_1. By properly arranging the geometry of the graphene blocks, we have successfully designed a graphene metasurface that can fulfill the polarization-switchable electromagnetic response mentioned above. When μ_c is 0.19 eV, the variation range of the reflection phase for the x-polarized incidence can be up to 4.9 rad in the interval of $w_1 \in$ [5 μm, 35 μm] and $l_2 \in$ [5 μm, 55 μm], while that for the y-polarized incidence is limited within 1.1 rad [Figs. 2(a) and 2(b)]. However, if μ_c is switched to 0.50 eV, the variation range of the reflection phase of the x-polarized incidence is smaller than 1.2 rad in the interval of $w_1 \in$ [5 μm, 35 μm] and $l_2 \in$ [5 μm, 55 μm], while that for the y-polarized incidence can reach 7.5 rad [Figs. 2(c) and 2(d)]. Therefore, a large phase coverage can be switched from x polarization to y polarization by changing the chemical potential of graphene from one value to another one. As μ_c is 0.19 and 0.50 eV, respectively, the reflection amplitudes for x- and y- polarized incidence are

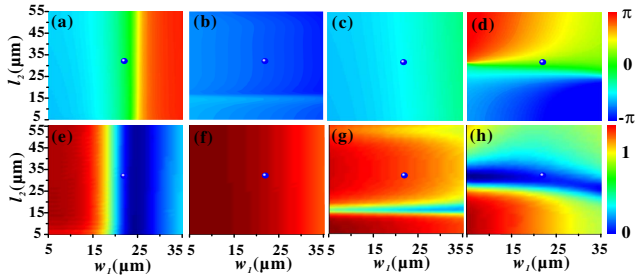

Fig. 2. Reflection phases (a)–(d) and amplitudes (e)–(h) for the x-polarized (a), (c), (e), (g) and y-polarized (b), (d), (f), (h) EWs versus w_1 and l_2, as μ_c is set at (a), (b), (e), f) 0.19 and (c), (d), (g), (h) 0.50 eV, respectively. In the simulations, p_x, p_y, d, l_1, w_2, l_a, and l_b are fixed at 55, 55, 50, 55, 11, 9.5, and 9 μm, respectively. The blue points in (a)–(h) correspond to $w_1 = 24$ and $l_2 = 32$ μm.

shown in Figs. 3(e)–3(h). To further understand the polarization-switchable optical response, we have presented the electric field intensity distributions in plane A and plane B [Figs. 3(a) and 3(b)] as the geometrical parameters of the metasurface correspond to the blue point in Fig. 2. As shown in Figs. 3(c)–3(f), merely the surface plasmon resonance mode of LGB can be excited as the metasurface is illuminated by the x-polarized incidence. This clearly indicates that the reflection phase of the x-polarized incidence can only be modulated by w_1 with $\mu_c = 0.19$ eV. As for RGB, it can only be excited under the y-polarized incidence with $\mu_c = 0.50$ eV, and contributes to shift the reflection phase by varying l_2 [Figs. 3(g)–3(j)].

By spatially tailoring the geometry of the metasurfaces in an array, one can design the phase discontinuity along the interface and realize the polarization-switchable wave-front manipulation as required. Assuming the metasurfaces are periodically arranged along the x direction, the reflected EWs are described as

$$\begin{cases} E_x^{\text{out}} = A_{x1}(x)e^{\text{i}f_{x1}(x)}E_x^{\text{in}} & (\mu_c = 0.19\ \text{eV}) \\ E_y^{\text{out}} = A_{y1}(x)e^{\text{i}f_{y1}(x)}E_y^{\text{in}} & (\mu_c = 0.19\ \text{eV}) \\ E_x^{\text{out}} = A_{x2}(x)e^{\text{i}f_{x2}(x)}E_x^{\text{in}} & (\mu_c = 0.50\ \text{eV}) \\ E_y^{\text{out}} = A_{y2}(x)e^{\text{i}f_{y2}(x)}E_y^{\text{in}} & (\mu_c = 0.50\ \text{eV}) \end{cases}, \quad (3)$$

where E_x^{in} (E_y^{in}) and E_x^{out} (E_y^{out}) represent the x- and y-polarized incident and reflected EWs, respectively, and $f_{hk}(x)$ and $A_{hk}(x)$ ($h = x, y; k = 1, 2$) are the phase and amplitude distributions with respect to the x axis that are introduced by the graphene metasurface, respectively. Due to the fact that the variation ranges of both of the x- and y- polarized reflection phases are far less than 2π at $\mu_c = 0.50$ eV [Fig. 2(c)] and 0.19 eV [Fig. 2(b)], $f_{x2}(x)$ and $f_{y1}(x)$ are nearly kept unchanged with respect to the x axis. Hence, the specular reflection occurs for the x- and y-polarized incidences at $\mu_c = 0.50$ and 0.19 eV, respectively. Meanwhile, if $f_{x1}(x)$ and $f_{y2}(x)$ are satisfied to follow the desired phase distributions for particular wave-front manipulation at $\mu_c = 0.19$ and 0.50 eV, the polarization-switchable functionalities are highly expectable. To validate the concept, we designed two metasurfaces for polarization-switchable wave-front manipulation applications including anomalous reflection and focusing.

Anomalous reflection can be realized by arranging metasurface array with a linear gradient phase at the interface of two different media. Hence, $f_{x1}(x)$ and $f_{y2}(x)$ should be designed to satisfy the following equations to work with switchable polarization:

$$f_{x1}(x), f_{y2}(x) = \varphi_0 + 2\pi/L_x x, \quad (4)$$

where φ_0 is a constant phase shift, and L_x is the lattice constant of the supercell. Here, seven metasurface units with different w_1 and l_2 are put side by side along the x direction to form a supercell so as to achieve the required phase distributions [w_1 and l_2 for each unit within a supercell are shown in Fig. 4(a)]. The reflection phase and amplitude of each unit within a supercell for the x- and y-polarized EWs are shown in Figs. 4(b) and 4(c). When μ_c is 0.19 eV, the reflection phase shift of the x-polarized incidence is linearly distributed and covers a large phase range of 4.9 rad, while that for the y-polarized incidence varies gently [Fig. 4(b)]. The reflection phase for the x- and y-polarized incidences is reversed as μ_c is switched to 0.50 eV [Fig. 4(c)]. The simulation results show that the x-polarized incidence is anomalously reflected with $\mu_c =$ 0.19 eV, while the y-polarized incidence is normally reflected [Figs. 4(d) and 4(e)]. In contrast, the field intensity distributions are reversed for the x- and y-polarized incidences as μ_c is switched to 0.5 eV [Figs. 4(f) and 4(g)]. Polarization-switchable focusing can be exploited by making $f_{x1}(x)$ and $f_{y2}(x)$ abide by a hyperboloidal profile as

$$f_{x1}(x), f_{y2}(x) = \varphi_{0f} + k_0\left(l_f - \sqrt{x^2 + l_f^2}\right) + 2m\pi. \quad (5)$$

Here, φ_{0f} is the initial phase shift at the center of the focusing lens ($x = 0$), l_f represents the focusing length, m is an arbitrary integer, and k_0 is the propagation constant of the EWs in free space. Forty-one metasurface units with different w_1 and l_2 are arranged along the x direction to form the polarization-switchable focusing lens with $l_f = 1000$ μm [w_1 and l_2 for each unit are shown in Fig. 5(a)]. The reflection phase

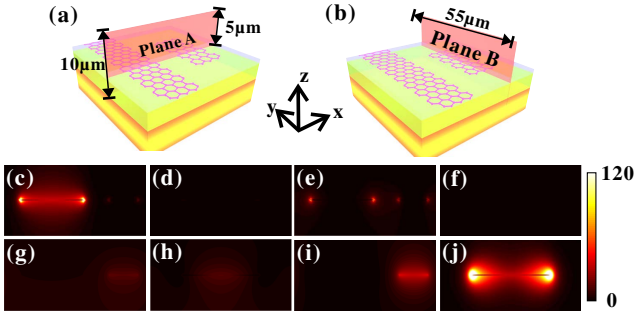

Fig. 3. (a), (b) Planes A and B are perpendicular to y and x directions, respectively, and located at the center of the unit cell along the x direction and the center of RGB along the y direction, respectively. The size of planes A and B are $55(x) \times 10(z)$ and $55\ \mu\text{m}(y) \times 10\ \mu\text{m}(z)$, respectively. (c)–(j) The simulated field intensity distribution of $|E|^2$ in (c), (e), (g), and (i) the plane A and (d), (f), (h), and (j) the plane B for the (c)–(f) x- and for (g)–(j) y-polarized EWs, as μ_c is set at (c), (d), (g), and (h) 0.19 and at (e), (f), (i), and (j) 0.50 eV, respectively. In the simulations, all the structural parameters of the metasurface are the same as those marked with the blue points in Fig. 2.

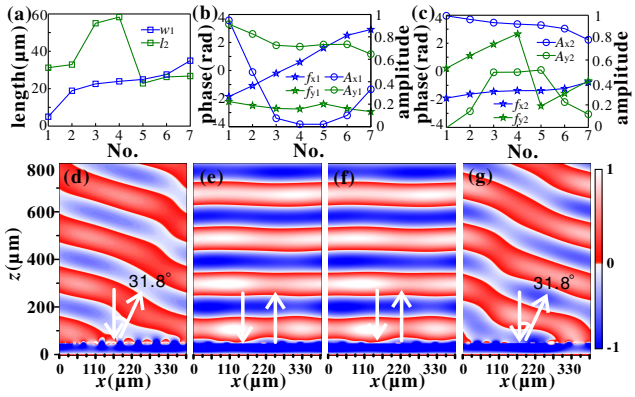

Fig. 4. (a) w_1 and l_2 for each unit within a supercell. (b), (c) The reflection phase and amplitude distributions for the x and y polarizations within a supercell of the designed beam deflector as μ_c is (b) 0.19 and (c) 0.5 eV, respectively. (d)–(g) The simulated distributions of the real part of (d), (f) E_x and (e), (g) E_y in the $x-z$ plane when illuminated with the (d), (f) x- and (e), (g) y-polarized EWs, respectively, at μ_c = (d), (e) 0.19 eV and (f), (g) = 0.5 eV.

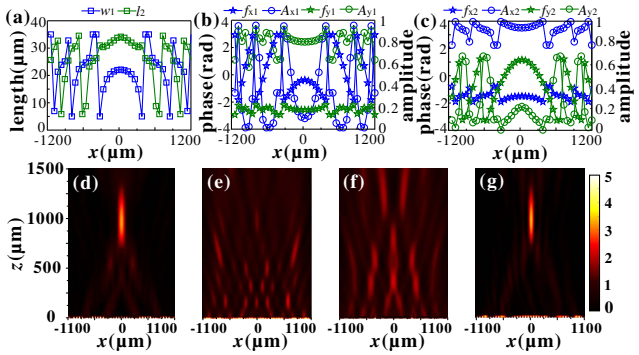

Fig. 5. (a) Distributions of w_1 and l_2. (b, c) The reflection phase and amplitude distributions for the x- and y- polarizations of the designed focusing lens as μ_c is (b) 0.19 eV and (c) 0.50 eV, respectively. (d)–(g) The simulated field intensity distributions of $|E|^2$ in the $x-y$ plane as the focusing lens are illuminated with the (d), (f) x- and (e), (g) y-polarized EWs at μ_c = (d), (e) 0.19 eV and = (f), (g) 0.50 eV, respectively.

distributions for the x-polarized incidence are hyperboloidal with $\varphi_{0f} = -0.41$ rad at $\mu_c = 0.19$ eV, while that for the y-polarized incidence fluctuates slightly between −2.73 and −2.39 rad [Fig. 5(b)]. The reflection phase distributions are reversed as μ_c is switched to 0.50 eV [Fig. 5(c)]. That is to say that, $f_{x1}(x)$ and $f_{y2}(x)$ are designed to follow the hyperboloidal distributions, while $f_{x2}(x)$ and $f_{y1}(x)$ are close to uniform distributions. Figs. 5(d)–5(g) show that the reflected electric field of the x- and y-polarized incidences are all focused at $z = 1000$ μm with $\mu_c = 0.19$ and $\mu_c = 0.50$ eV, respectively, while no clear focusing spot are found for the y- and x-polarized incidences with $\mu_c = 0.19$ and $\mu_c = 0.50$ eV, respectively. It is noted here that the electric field intensity distributions in Figs. 5(e) and 5(f) are supposed to be uniformly distributed, but actually are not absolutely uniform. This is attributed to the fact that the reflection phase is inevitably influenced by the metasurface, and the finite size is used for the lens.

In conclusion, we proposed a novel graphene metasurface to produce polarization-switchable electromagnetic response. We have demonstrated that the phase shifts covering a large phase range can be switched from x polarization to y polarization by tuning the chemical potential of graphene. Typical wave-front manipulation applications, including polarization-switchable anomalous reflection and focusing, have been numerically demonstrated. The presented results provide a fire-new design concept for polarization-controllable devices and can lead to various new applications in nanophotonics, such as polarization-switchable polarization beam splitting, image sensing, and dynamically generating complex light field.

Funding. National Natural Science Foundation of China (11474116, 11674118).

REFERENCES

1. N. Yu, P. Genevet, M. A. Kats, F. Aieta, J.-P. Tetienne, F. Capasso, and Z. Gaburro, Science **334**, 333 (2011).
2. M. Khorasaninejad, W. T. Chen, R. C. Devlin, J. Oh, A. Y. Zhu, and F. Capasso, Science **352**, 1190 (2016).
3. E. Karimi, S. A. Schulz, I. De Leon, H. Qassim, J. Upham, and R. W. Boyd, Light Sci. Appl. **3**, e167 (2014).
4. G. Zheng, H. Mühlenbernd, M. Kenney, G. Li, T. Zentgraf, and S. Zhang, Nat. Nanotechnol. **10**, 308 (2015).
5. X. Zang, F. Dong, F. Yue, C. Zhang, L. Xu, Z. Song, M. Chen, P.-Y. Chen, G. S. Buller, Y. Zhu, S. Zhuang, W. Chu, S. Zhang, and X. Chen, Adv. Mater. **30**, 1707499 (2018).
6. J. P. Balthasar Mueller, N. A. Rubin, R. C. Devlin, B. Groever, and F. Capasso, Phys. Rev. Lett. **118**, 113901 (2017).
7. A. Arbabi, Y. Horie, M. Bagheri, and A. Faraon, Nat. Nanotechnol. **10**, 937 (2015).
8. K. E. Chong, I. Staude, A. James, J. Dominguez, S. Liu, S. Campione, G. S. Subramania, T. S. Luk, M. Decker, D. N. Neshev, I. Brener, and Y. S. Kivshar, Nano Lett. **15**, 5369 (2015).
9. X. Kong, J. Xu, J.-J. Mo, and S. Liu, Front. Optoelectron. **10**, 124 (2017).
10. C. H. Chu, M. L. Tseng, J. Chen, P. C. Wu, Y.-H. Chen, H.-C. Wang, T.-Y. Chen, W. T. Hsieh, H. J. Wu, G. Sun, and D. P. Tsai, Laser Photon. Rev. **10**, 986 (2016).
11. K. Thyagarajan, R. Sokhoyan, L. Zornberg, and H. A. Atwater, Adv. Mater. **29**, 1701044 (2017).
12. J. Park, J.-H. Kang, S. J. Kim, X. Liu, and M. L. Brongersma, Nano Lett. **17**, 407 (2017).
13. O. Buchnev, N. Podoliak, M. Kaczmarek, N. I. Zheludev, and V. A. Fedotov, Adv. Opt. Mater. **3**, 674 (2015).
14. D. Franklin, Y. Chen, A. Vazquez-Guardado, S. Modak, J. Boroumand, D. Xu, S.-T. Wu, and D. Chanda, Nat. Commun. **6**, 7337 (2015).
15. H. Cheng, S. Chen, P. Yu, W. Liu, Z. Li, J. Li, B. Xie, and J. Tian, Adv. Opt. Mater. **3**, 1744 (2015).
16. T. Yang, H. Lin, and B. Jia, Front. Optoelectron. **11**, 2 (2018).
17. W. Zhu, Q. Song, L. Yan, W. Zhang, P.-C. Wu, L. K. Chin, H. Cai, D. P. Tsai, Z. X. Shen, T. W. Deng, S. K. Ting, Y. Gu, G. Q. Lo, D. L. Kwong, Z. C. Yang, R. Huang, A.-Q. Liu, and N. Zheludev, Adv. Mater. **27**, 4739 (2015).
18. K. Chen, Y. Feng, F. Monticone, J. Zhao, B. Zhu, T. Jiang, L. Zhang, Y. Kim, X. Ding, S. Zhang, A. Alù, and C.-W. Qiu, Adv. Mater. **29**, 1606422 (2017).
19. P. B. Johnson and R.-W. Christy, Phys. Rev. B **6**, 4370 (1972).
20. Y.-S. Jin, G.-J. Kim, and S.-G. Jeon, J. Korean Phys. Soc. **49**, 513 (2006).